PROCEEDINGS OF MOSES2023 CONFERENCE
4TH INTERNATIONAL CONFERENCE ON MODELLING AND OPTIMISATION OF SHIP ENERGY SYSTEMS
26-27 OCTOBER 2023, DELFT, NETHERLANDS

Thermodynamic Evaluation of a Combined SOFC-PEMFC Cycle System

N.G.H. Goselink[a,*], B.J. Boersma[a], and L. van Biert[a]

[a]Delft University of Technology, Delft, The Netherlands
[*]n.g.h.goselink@tudelft.nl

Abstract

Solid oxide fuel cell (SOFC) technology offers a promising way to reduce maritime greenhouse gas (GHG) emissions. Integration with a proton exchange membrane fuel cell (PEMFC) allows unreacted hydrogen, produced in the SOFC stack, to be reused and increase the electrical efficiency of the system. In this study, the Cycle Tempo software is used to model a SOFC-PEFMC combined cycle system operating on methane. The system is thermodynamically analysed to reveal the influence of SOFC fuel utilisation, cell voltage, operating temperature and PEMFC cell voltage on the system performance. A multivariable parametric analysis is applied to generate contour plots of net electrical efficiency and fraction of total power produced by the PEMFC. The analysis shows that increasing the cell voltage of both the SOFC and PEMFC has a positive influence on efficiency, whereas increasing the fuel utilisation reduces the system efficiency. Efficiencies in the range of 50-68% can be achieved. Model assumptions for PEMFC operating parameters are verified to exert little influence on the system efficiency, which confirms the assumption of constant values for these parameters. This study highlights the high-efficiency potential of the combined system and the difficulties that arise from thermally integrating an SOFC with a PEMFC.

Keywords: SOFC; PEMFC; Combined cycle system; Thermodynamic analysis.

1 INTRODUCTION

The maritime industry is responsible for roughly three percent of global anthropogenic greenhouse gas (GHG) emissions [1]. Therefore, the International Maritime Organisation (IMO) has imposed several guidelines and regulations to achieve net-zero GHG emissions by 2050 [2]. Solid oxide fuel cells (SOFC) have been recognized as a promising technology for use on board ships [3]. The SOFC can achieve efficiencies of up to 60% in a stand-alone configuration [4], [5], which is significantly higher than that of conventional internal combustion engines and gas turbines, as reported in [6]. In addition, the internal reforming capabilities of the SOFC make the system suitable for a variety of alternative fuels, such as methanol, ammonia, hydrogen or (L)NG, while emitting little to no NO_x and SO_x [7].

The stand-alone efficiency of an SOFC is already high at 60% but can be further increased by reusing the fuel and heat within the anode/cathode off-gas streams [8], [9]. Integrating a pressurized SOFC with a gas turbine (GT) increases the net electrical efficiency to 70% [10]. However, direct coupling between the SOFC and gas turbine requires matching of operating points, limiting the system operating envelope and introducing significant control challenges [11]. Another approach is the addition of an internal combustion engine (ICE). The SOFC-ICE combined system can theoretically achieve similar efficiencies ($\sim$70%), with the added benefit of improved transient capabilities and better part-load performance [12], [13] compared to SOFC-GT systems. However, the direct combustion of residual fuel still generates significant amounts of emissions such as NO_x.

More recently, the combination of an SOFC and proton exchange membrane fuel cell (PEMFC) has surfaced as a viable alternative. This approach benefits from both energy generation and hydrogen production within the SOFC. Because the fuel utilisation is smaller than unity, ranging from 0.60 to 0.90, a significant amount of unreacted hydrogen is present in the anode off-gas stream. This hydrogen can be used in a PEMFC to generate additional electricity, thereby increasing the overall system efficiency [14], [15]. In addition to H_2, the syngas includes major species such as CO, CO_2 and H_2O. Because the PEMFC has a limited CO tolerance, a few parts per million (ppm) can already cause cell performance degradation [16], this component must

DOI: https://doi.org/10.59490/moses.2023.659

be removed from the syngas stream. The commonly applied approaches are water gas shift (WGS), preferential oxidation (PrOX) and pressure swing adsorption (PSA) [6]. The combined SOFC-PEMFC cycle system is reported to be potentially competitive with other combined cycle systems in terms of efficiency [17]. However, because this specific system layout remains relatively unstudied, a structured review of its performance potential is lacking. This represents the knowledge gap that this study aims to address.

Thermodynamic analysis is an established approach to compare the efficiency of combined system architectures with stand-alone SOFCs or between different combined cycles. However, because most thermodynamic analyses are performed at arbitrary design points, it is difficult to compare these systems. Therefore, van Biert et al. [9] investigated the thermodynamic efficiencies of four different solid oxide fuel cell-combined cycle system across their entire operating envelope. The selected systems were a steam turbine combined cycle, two gas turbine combined cycles at ambient and elevated pressure, and a reciprocating engine combined cycle. The operating parameters, e.g., fuel utilization, cell voltage and stack temperature are varied to achieve more meaningful results, as the stack operating parameters are similar for all cases investigated.

To investigate the performance potential of the SOFC-PEMFC combined cycle system, this study follows a similar approach, by analysing the systems' efficiency across an operating envelope of typical SOFC operating parameters. To the best of the authors knowledge, this is the first time that such a complete analysis of the SOFC-PEMFC system performance is performed.

The proposed configuration is presented and modeled in sections 2-3. The results of the multivariable parameter analysis are analysed and discussed in section 4. Finally, the conclusions of the preliminary analysis are presented in section 5 and future work is discussed in 6. This work will thus present a basis for the comparison of the SOFC-PEMFC combined cycle performance with other combined cycle systems and stand-alone configurations.

2 CONFIGURATION OF THE PROPOSED SOFC-PEMFC COMBINED CYCLE

A schematic of the SOFC-PEMFC combined cycle system is shown in figure 1. The system consists of different modules: the SOFC subsystem, gas cleaning equipment and PEMFC subsystem.

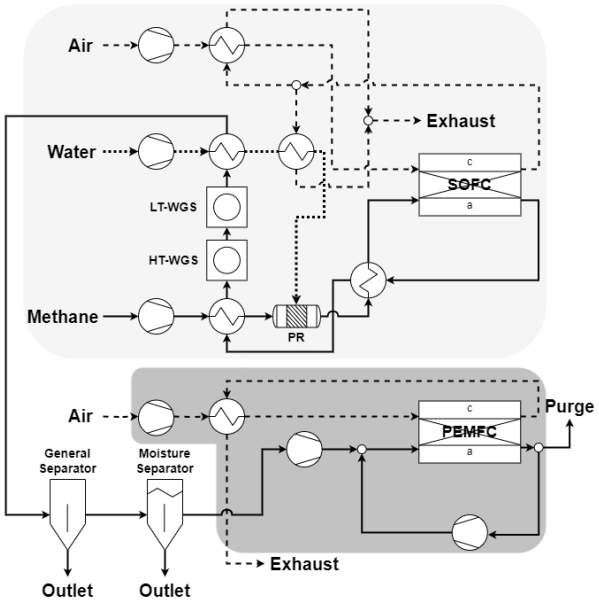

Figure 1: SOFC-PEMFC combined cycle system layout

The SOFC layout is based on the configuration reported by Riensche et al. [18]. Air is supplied by a compressor to overcome the pressure losses in the system and is preheated before it enters the SOFC cathode. The fuel, in this case methane, is compressed, preheated, and partly reformed in a pre-reformer (PR) before it is fed to the anode side. Within the pre-reformer, methane steam reforming and water gas shift reactions convert methane into hydrogen. A pre-reforming temperature of 450°C is chosen, such that it matches the pre-reformer outlet temperature. A pre-reform ratio of 20% is assumed, the minimum amount as specified by a SOFC manufacturer [19]. The anode and cathode off-gas (AOG) and (COG) are reused to preheat the reactant flows. The COG is used to preheat the airflow and superheat the water. In contrast to the stand-alone case, the AOG is not recirculated and burnt but is used to directly preheat the fuel and evaporate the water. Subsequently, the AOG is cleaned and purified such that the remaining chemical energy contained within the hydrogen-rich gas is converted into electricity in the PEMFC. The generated steam is used for methane reforming and water gas shift processes. A steam-to-carbon ratio (S/C), the ratio of moles of steam to moles of carbon at the anode inlet, of 2.25 is assumed to prevent the formation of solid carbon inside the SOFC [20]. The AOG is cleaned to remove CO, CO_2, and H_2O before it can be fed to the PEMFC. CO removal is achieved in a high- and low-

temperature water gas shift (WGS) reactor (350 and 180°C respectively) [21]. At higher temperatures, the kinetics are faster, whereas at lower temperatures the H_2 yield is larger and the equilibrium concentration of CO is lower [6]. Because WGS alone cannot meet the requirement of CO $<$ 10 ppm [22], another purification step is required to remove the remaining trace CO. Various methods are available for this purpose. However, because the identification and analysis of the most suitable method is outside the scope of this research, a general separator is assumed. This component is modeled to remove 99.5 mole % CO_2 and all the remaining CO. In the last step, water vapor is separated from the gas flow in a moisture separator. The purified gas flow (designated H_2 in figure 2) contains a high concentration of hydrogen and small concentrations of impurities and water vapor. The compositions of the different process flows shown in figures 1 and 2, are listed in table 1.

For the PEMFC subsystem model, a simple architecture is assumed that consists of a water-cooled stack operating at 60°C, fed with reactant flows at 40°C. The air is compressed and preheated by residual heat in the PEMFC COG stream before entering the cathode. The hydrogen-rich gas flow is cooled to 40°C before being compressed, such that it can be directly connected to the anode side. Because the fuel utilisation in the PEMFC is lower than unity (85% under nominal conditions), the anode off-gas is recirculated and mixed with fresh gas at the anode inlet. Consequently, CO_2 in the anode gas stream might accumulate in the system. While CO_2 itself is inert, the reverse WGS reaction can create CO in such amounts (CO $>$ 10ppm) that it can poison the anode, thereby reducing the stack efficiency. To remove this CO_2, a continuous purge is modeled, that vents 20% of the anode off-gas to the environment. This maintains the level of CO_2 at the anode inlet at such a level that the performance degradation is less than 5% under nominal conditions [23]. Because purging hydrogen also introduces system losses, the chosen value of 20% represents an efficiency trade-off.

3 METHODOLOGY

The flow-sheet program *Cycle-Tempo*, an in-house software developed at TU Delft, is used for the thermodynamic evaluation of this system. The program contains a library of components such as a pump, compressor, fuel cell stack, reformer, combustor and heat exchangers. Combining these, a complete fuel cell system is created. In Cycle-Tempo, these components form a system matrix consisting of mass and energy equations, which are solved to determine the pressure, mass flow, temperature and flow composition of each component. The results can be used to analyse the performance of power plants, for example, the system efficiency and exergy analysis [24]. This modeling software is commonly used in SOFC-based power plant research [25]–[27]. The model assumptions and governing equations for the different subsystems are given below. Cycle-Tempo employs a Gibbs free energy minimisation routine for equilibrium calculations in the cell models.

3.1 Model assumptions

1. Pressure drops over the pipes are neglected.
2. The system operates in steady-state.
3. The fuel cell, heat exchanger and chemical reactor components are all assumed to be well insulated. There is no heat transfer between those components and the ambient.
4. Humidification of the PEMFC cathode is not included.
5. 99.5 Mole % of CO_2 is removed from the AOG in the general separator.
6. 100 Mole % of CO is removed from the AOG in the general separator.

3.2 SOFC model

The SOFC module uses the mole flow and conditions (composition and temperature) at the cell inlet to calculate the outlet mole flows and conditions. The operating point of the fuel cell is defined by specifying the power generation $P_{el,AC}$ and the cell voltage V_{cell}. The other parameters such as current I and power generated by the stack $P_{el,DC}$ are calculated from the input data. These processes are assumed to occur at constant internal pressure, gas composition and temperature. The required fuel mass flow at the anode inlet m_a^{in} is calculated from the total current I, and fuel utilisation u_f, according to [25]

$$m_a^{in} = \frac{IM_a}{2F(y_{H_2}^{in} + y_{CO}^{in} + 4_{CH_4}^{in})u_f} \qquad (1)$$

where, y_i^{in} is the anode gas concentrations at the inlet, M_a the molar mass of the anode gas and F is the Faraday constant. The oxygen mass flow from the cathode to the anode $m_{O_2,c\to a}$ is also calculated

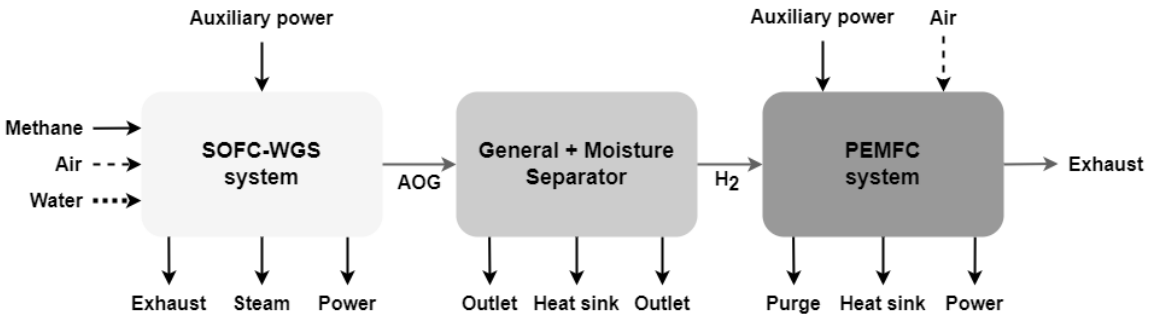

Figure 2: Schematic of the energy inputs and outputs of the SOFC-PEMFC combined system. AOG represents the anode off-gas of the SOFC, that is being cleaned to generate a high-purity hydrogen mixutre (H_2 stream).

from the total current I,

$$m_{O_2,c\to a} = M_{O_2}\frac{I}{4F} \tag{2}$$

where M_{O_2} is the oxygen molar mass. The cathode mass flow is determined from the energy balance over the fuel cell because the temperature at the outlet is an input and the anode and cathode outlet temperatures are assumed to be identical.

A simplified isothermal model is used for the fuel cell, to limit the computational time and convergence to acceptable levels for flow sheeting modeling purposes. The fuel cell model calculates the local processes along the direction of the flow, with all processes occurring at a constant temperature T. Internal profiles are obtained for the concentrations and current density to determine the local reversible voltage. To calculate these profiles, the cell is discretised in the direction of the flow such that pressure and gas composition are assumed constant in the cross-section perpendicular to the flow. The position of the local variables along the profiles is indicated by subscript x. The reversible, no loss, voltage $V_{rev,x}$ is calculated according to [25]:

$$V_{rev,x} = V^0_{rev} + \frac{\bar{R}T}{2F}\ln\left\{\frac{y^{1/2}_{O_2,c}y_{H_2,a}}{y_{H_2O,a}}\times p^{1/2}_{cell}\right\} \tag{3}$$

with standard reversible voltage V^0_{rev}, universal gas constant $\bar{R}$, temperature T, mole fraction y and pressure p_{cell}. In reality, irreversibilities that occur within the cell will result in a cell voltage, V_x, smaller than the reversible voltage. This difference is indicated by the voltage loss ΔV_x. Because the model assumes that the voltage losses are negligible at the electrode level in the x-direction, the cell voltage is assumed to be constant over the fuel cell:

$$V = V_x = V_{rev,x} - \Delta V_x \tag{4}$$

The current density in the flow direction along the cell is:

$$i_x = \frac{\Delta V_x}{R_{eq}} \tag{5}$$

where R_{eq} denotes the equivalent cell resistance. Therefore, for the entire cell, the total current I is calculated according to:

$$I = \frac{u_f A}{R_{eq}\int_0^{u_f} d\lambda/(V_{rev}-V)} \tag{6}$$

Table 1: Composition of SOFC-PEMFC system process flows

Gas stream	**Composition [mole %]**
Methane	CH_4=100%
Air	Ar=0.92%, CO_2=0.03%, H_2O=1.01%, N_2=77.29%, O_2=20.75%
Water	H_2O (l)=100%
AOG	H_2O=66.29% , CO_2=17.72%, H_2=13.72%, CO=2.26%
H_2	H_2O=7.29%, CO_2=0.58%, H_2=92.14%
SOFC exhaust	Ar=0.95%, CO_2=0.03%, H_2O=1.05%, O_2=17.98%, N_2=79.99%
PEMFC exhaust	Ar=0.82%, CO_2=0.03%, H_2O=20.93%, O_2=9.26%, N_2=68.96%
PEMFC purge	CH_4=0.12%, CO_2=15.55%, H_2=84.32
General separator outlet	CO=0.01%, CO_2=99.99%
Moisture separator outlet	H_2O (l)=100%

where A is the cell area and λ is the dimensionless reaction coordinate. The cell power can be calculated using the known current and voltage.

The system operates on pure methane, CH_4, of which 20% is bypassed to be converted externally in an adiabatic pre-reformer. The remaining methane is converted internally in the SOFC into a hydrogen-rich gas. Methane reforming occurs through steam reforming and the water gas shift reaction (Eqs. 7 and 8).

$$\mathrm{CH_4 + H_2O \rightleftarrows CO + 3\,H_2} \tag{7}$$

$$\mathrm{CO + H_2O \rightleftarrows H_2 + CO_2} \tag{8}$$

The steam reforming reaction requires water, which is vaporised by heat recovered from the SOFC exhaust stream.

3.3 SOFC anode off-gas cleaning model

In WGS reactors, the equilibrium water gas shift reaction occurs (Eq. 8). The equilibrium is calculated by means of the equilibrium constant K_{react}, as a function of temperature T_{react}, according to

$$K_{react} = \frac{(\partial p_{CO_2} + y)(\partial p_{H_2} + y)}{(\partial p_{CO} - y)(\partial p_{H_2O} - y)} \tag{9}$$

where y is the reaction coordinate of the water gas shift reaction and ∂p_x is the partial pressure of component x. The outlet temperature and gas composition are calculated using equilibrium, energy and mass balances.
The flow is subsequently cooled in the moisture separator, where condensation occurs and is separated via a separate pipe.

3.4 PEMFC model

The PEMFC module calculations followed an approach similar to that described in Section 3.2, for the SOFC module. Only this time, the fuel mass flow is specified instead of the power generation. For low-temperature fuel cells, it is assumed that only H_2 is present in the fuel and that a shift reaction does not occur. Equation 2 can be rewritten as follows:

$$I = \frac{m_{a,in}}{M_a} 2F y^0_{H_2} u_f \tag{10}$$

The PEMFC is modeled with a cooling circuit, which is assumed to be under environmental conditions at the inlet of the pump (20°C, p_{amb}=1.103 bar).

3.5 System analysis

The main performance metric is the net electrical efficiency of the combined system, $\eta_{el,AC}$, which is calculated as

$$\eta_{el,AC} = \frac{P_{el,tot} - P_{aux}}{m_f LHV_{CH_4}} \tag{11}$$

In Equation 11, $P_{el,tot}$ is the net electrical power output of the system, calculated from the direct current (DC) power produced by both the SOFC and PEMFC, multiplied by the efficiency of converting DC into AC according to:

$$P_{el,tot} = (P_{SOFC,_{DC}} + P_{PEMFC,_{DC}})\eta_{DC/AC} \tag{12}$$

In addition, P_{aux} is defined as the total power consumption of all auxiliary components, such as pumps and compressors used in both the SOFC and PEMFC systems. The net electrical efficiency is calculated based on the lower heating value (LHV) of methane.

An additional metric of interest is the fraction of the total power delivered by the PEMFC, defined as

$$f_{P,_{PEMFC}} = \frac{P_{PEMFC,_{AC}}}{P_{PEMFC,_{AC}} + P_{SOFC,_{AC}}} \tag{13}$$

An overview of the operating parameters used in this study is provided in table 2.

3.6 Model verification

Figure 2 shows a schematic overview of the energy inputs and outputs of the combined cycle system. The SOFC and WGS reactors are integrated because the heat of the exothermic WGS reaction is used to evaporate the water required for the steam reforming reaction in the SOFC system. In figure 2, AOG stands for the anode off-gas stream and syngas containing residual hydrogen. The H_2 stream represents a high-purity hydrogen stream, which is suitable for fueling the PEMFC.

Model verification can be achieved at various levels. In this study, the energy balance of the complete system is calculated as a verification method. The SOFC power output is set to $P_{el,AC}$ = 200 kW, with the input parameters as presented in table 2, resulting in a PEMFC power output of $P_{el,AC}$ = 48,29 kW. It is verified that all components assumed adiabatic (e.g., nodes, reactors, heat exchangers) have zero energy losses.

Table 2: Input parameters used for analysis of the combined cycle system

Parameter	Value
General	
Heat exchanger pressure drop, Δp_{HEX}	0.05 [bar]
Economiser pressure drop, Δp_{ECO}	0.5 [bar]
Isentropic efficiency compressor, η_{is}	0.7 [-]
Mechanical efficiency compressor, η_{me}	0.8 [-]
DC-AC converter efficiency, $\eta_{converter}$	0.95 [-]
SOFC	
Average stack temperature, $T_{stack,SOFC}$	700 [°C]
Stack inlet temperature, $T_{in,SOFC}$	$T_{stack,SOFC}$ -50 [°C]
Stack outlet temperature, $T_{out,SOFC}$	$T_{stack,SOFC}$ +50 [°C]
Anode pressure drop, Δp_{an}	0.03 [bar]
Cathode pressure drop, Δp_{ca}	0.05 [bar]
Power output, $P_{SOFC,AC}$	200 [kW]
Operating pressure, p_{SOFC}	1.013 [bar]
Pre-reformer temperature, T_{reform}	450 [°C]
Syngas cleaning	
HT-WGS reaction temperature, T_{HT-WGS}	350 [°C]
LT-WGS reaction temperature, T_{LT-WGS}	180 [°C]
Fraction of CO separated, χ_{CO}	100 [mole %]
Fraction of CO_2 separated, χ_{CO_2}	99.5 [mole %]
PEMFC	
Average stack temperature, $T_{stack,PEMFC}$	60 [°C]
Anode pressure drop, Δp_{an}	0.03 [bar]
Cathode pressure drop, Δp_{ca}	0.03 [bar]
Operating pressure, p_{PEMFC}	1.013 [bar]
Fuel utilisation, u_f	0.85 [-]
Oxygen utilisation, u_{ox}	0.5 [-]
Anode purge percentage x_{purge}	20 [%]

Moreover, comparing the energy inputs and outputs, an absolute error of 0.01 kW and a relative error of 0.05% is observed. This is considered negligible small, such that the system is assumed to be verified for the energy balance.

4 RESULTS

The performance of the combined SOFC-PEMFC system is first evaluated for the nominal operating conditions of the SOFC power output of P_{SOFC} = 200 kW, under nominal conditions (table 3). This results in a methane mass flow rate of 0.00781 kg/s. The power output of the PEMFC is dependent on the amount of H_2 present in the SOFC anode off-gas stream. For the nominal operating point, the resulting hydrogen flow reads 0.00079 kg/s, producing 48.29 kW of PEMFC power. The total net power generated by the system $P_{el,tot}$ = 200 + 48.29 = 248.29 kW. The net efficiency is $\eta_{el,AC}$ = 59.7% and the fraction of power produced by the PEMFC is $f_{P,PEMFC}$ = 0.19 [-].

4.1 Multivariable parametric analysis

The SOFC-PEMFC system is subjected to a parametric analysis of typical SOFC and PEMFC operating variables. For the SOFC, the cell voltage is varied in the range 0.6-0.8 V, the fuel utilisation in the range 0.6-0.9 [-] and the stack temperature is between 600-900 °C; for the PEMFC, the cell voltage is varied in the range 0.6-0.8 V, while the stack temperature is kept constant. The analysis is performed with a finite parameter interval, the details are provided in table 3.

Table 3: Overview of the parameters varied in the analysis, with their respective range, interval and nominal values.

Parameter	Range	Interval	Nominal value
$V_{cell,SOFC}$ [V]	0.6-0.8	0.025	0.7
u_f [-]	0.6-0.9	0.025	0.8
$T_{stack,SOFC}$ [°C]	600-900	50	700
$V_{cell,PEMFC}$ [V]	0.6-0.8	0.025	0.7

4.1.1 SOFC cell voltage

Figure 3a shows the contours of net electrical efficiency and the fraction of total power delivered by the PEMFC for various SOFC fuel utilisations and cell voltages at a constant SOFC stack temperature of 700°C and PEMFC cell voltage of 0.7 V. At lower fuel utilisation levels, the fuel flow increases for a constant power output, enhancing the cooling effect owing to the internal reforming process. Therefore, less air is required to cool the stack such that the airflow is reduced, which negatively affects the waste thermal energy available in the cathode off-gas. This trend is accelerated at higher cell voltages because less waste heat is available owing to the reduction in electrochemical losses in the fuel cell. Consequently, the cathode off-gas stream does not contain sufficient thermal energy to preheat the cathode air stream and superheat the water stream. Hence, the system is unable to sustain itself which represents an invalid operating point. The entire invalid operating regime is indicated by the gray area in figure 3a. Within the valid operating envelope, the system efficiency is primarily affected by the cell voltage, whereas it only slightly increases for a decrease in fuel utilisation. The electrochemical losses in the SOFC are reduced by increasing the cell voltage. The required airflow is reduced by reducing the fuel utilisation, lowering the power consumption of the air compressors. Because the air compressor is the primary power consumer, the net electrical efficiency of the system is increased. The fraction of the total power produced by the PEMFC is primarily affected by fuel utilisation as the hydrogen availability for the PEMFC is increased for higher fuel flows. The influence of cell voltage is less prominent. The $f_{P_{PEMFC}}$ slightly reduces with an increase in cell voltage because less fuel is required to achieve the

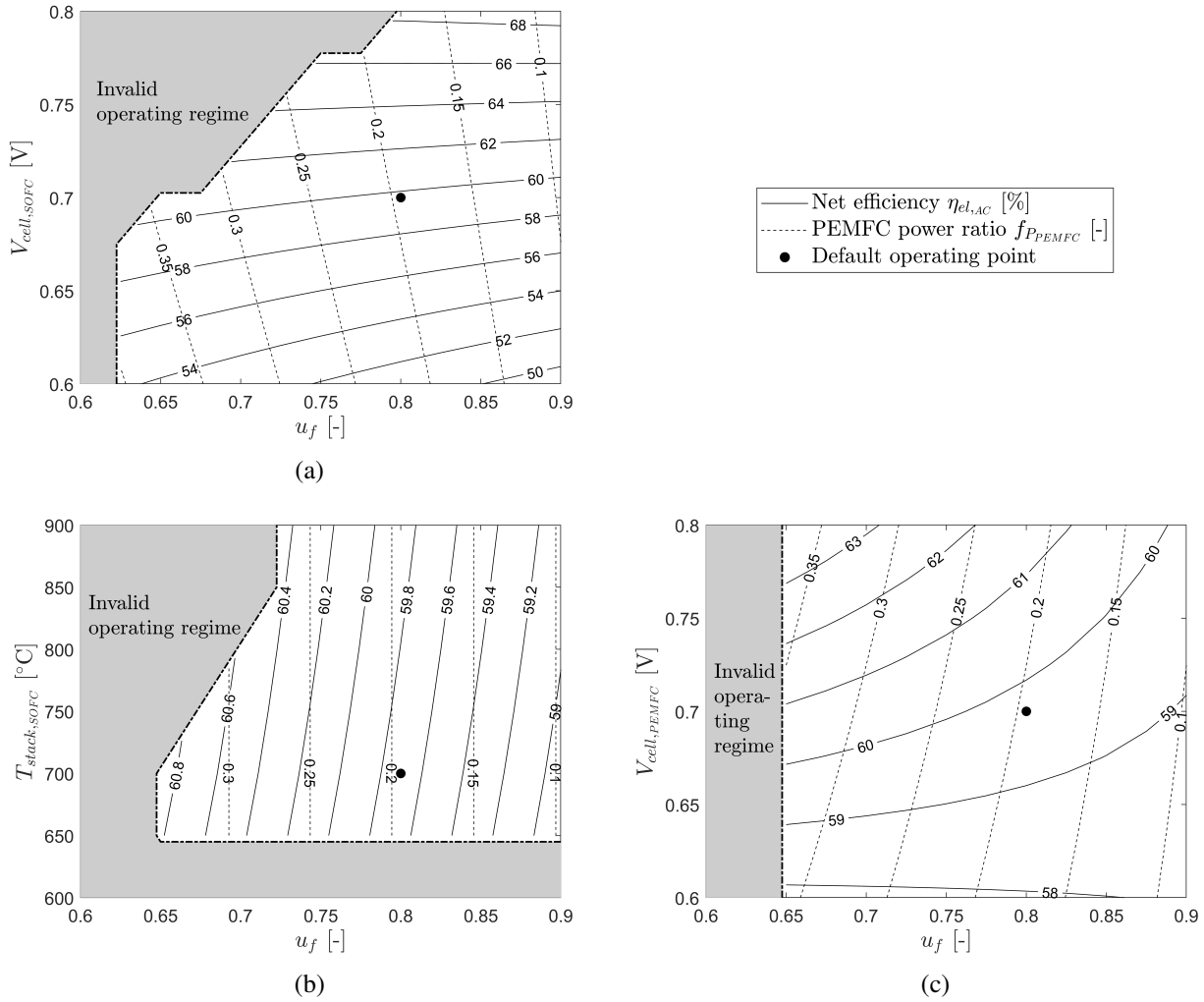

Figure 3: Contour plots of net electrical efficiency and fraction of power delivered by the PEMFC for various SOFC fuel utilisations, SOFC cell voltage (3a), SOFC stack temperature (3b) and PEMFC cell voltage (3c) at a constant PEMFC stack temperature of 60°C

same power output at higher cell efficiency. The maximum net electrical efficiency is 68.8%, for a cell voltage of 0.8 V and fuel utilisation of 0.9 [-]. This corresponds to the minimum PEMFC power production ratio of 0.085 [-].

4.1.2 SOFC stack temperature

Figure 3b shows contours of net electrical efficiency and the fraction of total power delivered by the PEMFC for various SOFC fuel utilisations and SOFC stack temperatures, at a constant SOFC cell voltage of 0.7 V and PEMFC cell voltage of 0.7 V. At $u_f < 0.65$ [-], the cathode off-gas did not contain sufficient thermal energy to sustain stable operation. In this case, this trend is enhanced by increasing the stack temperature, because less air is required for cooling. Owing to the reduction in the cathode mass flow, insufficient energy is available to preheat the airflow and superheat the water. Furthermore, the invalid operating regime extends over the entire range of u_f values, for $T_{stack_{SOFC}} < 650$°C. At these low temperatures, the anode off-gas does not contain sufficient thermal energy to preheat the fuel flow and evaporate the water stream. Increasing the stack operating temperature has a negligible effect on the system efficiency and power production ratio. Because operational conditions imposed on the stack, such as the operating temperature and pressure, do not affect the cell voltage, this does not affect the stack efficiency. This behaviour deviates from reality, where an increase in temperature will result in decreased voltage losses and an increased efficiency. Nonetheless, a marginal efficiency increase is observed for increasing SOFC stack temperatures, as less cooling air is required, reducing the auxiliary power consumption. The fraction of total power produced by the PEMFC is only seen to increase with a reduction in fuel util-

isation, as more hydrogen is available to be fed to the PEMFC. The maximum net electrical efficiency ($\eta_{el_{AC}}$ = 60.9%) is achieved for medium-low stack temperatures (650-700°C) and low fuel utilisation levels.

4.1.3 PEMFC cell voltage

Figure 3c displays contours of net electrical efficiency and fraction of the total power produced by the PEMFC as a function of SOFC fuel utilisation and PEMFC cell voltage, for a constant SOFC cell voltage of 0.7 V and SOFC stack temperature of 700°C. A fuel utilisation factor of 0.65 limits the valid operating regime. Because the electrical efficiency is seen to increase with an increase in the PEMFC cell voltage and a decrease in SOFC fuel utilisation, the maximum efficiency ($\eta_{el_{AC}} \approx 64\%$) is achieved for the maximum cell voltage and minimum fuel utilisation. At lower PEMFC cell voltages ($V_{cell_{PEMFC}}$ <0.625 V), this trend is reversed. The electrical efficiency decreases with a decrease in fuel utilisation. This is because of the increased hydrogen flow to the PEMFC, which increases the auxiliary power demand of the PEMFC system. This trend is further enhanced by the reduction in PEMFC efficiency with increased electrochemical losses. Because the SOFC operating parameters are kept constant in this case, the increase in net electrical efficiency follows directly from an increase in the PEMFC efficiency, combined with an increase in the PEMFC power output. The fraction of total power produced by the PEMFC primarily increases with a reduction in fuel utilisation and only slightly with an increase in the PEMFC cell voltage.

4.2 Sensitivity analysis

The PEMFC operating parameters that were kept constant during the foregoing analysis are investigated to analyse their influence on the system performance. The parameters investigated are the anode purge percentage x_{purge} as well as the fuel utilisation $u_{f,PEM}$. The influence of these parameters on the net electrical efficiency $\eta_{el,AC}$ and the fraction of power delivered by the PEMFC $f_{P_{PEMFC}}$ is presented in table 4. For every parameter, the nominal values and variations are provided. The last two columns provide the percentage changes according to

$$\text{Percentage change} = \frac{X_{new} - X_{nominal}}{X_{nominal}} \times 100\% \tag{14}$$

with X representing the system performance indicators $\eta_{el,AC}$ and $f_{P_{PEMFC}}$.

Both the PEMFC purge percentage and fuel utilisation are verified to have little influence on the system efficiency. At x_{purge}=0 and $u_{f,PEM}$=0.9, the net electrical efficiency is 60.3%, which is only slightly higher that under nominal conditions. The influence on the PEMFC power production is larger. As expected, the power produced by the PEMFC is directly influenced by the fuel utilisation and purge percentage. Nonetheless, varying these parameters did not change the conclusions presented in this study. Owing to the lack of physical feedback from the PEMFC to the SOFC, the PEMFC can be optimised without affecting the SOFC performance. Based on these observations, the assumed constant parameter values are considered acceptable.

5 CONCLUSION

A thermodynamic analysis of the SOFC-PEMFC combined cycle system is presented in this paper. The SOFC fuel utilisation, cell voltage and operating temperature were varied in addition to the PEMFC cell voltage. The calculated net electrical efficiency $\eta_{el_{AC}}$, varies in the range of 50-68%. The net electrical efficiency increases with SOFC and PEMFC cell voltages as electrochemical losses are reduced. The efficiency further increases with a decrease in SOFC fuel utilisation, as less air is required to cool the stack. The fraction of the total power produced by the PEMFC is seen to decrease with an increase in SOFC cell voltage and fuel utilisation, as the SOFC losses are reduced and less hydrogen is available for the PEMFC. An increase in the PEMFC cell voltage results in an increase in the power produced by the PEMFC. This analysis shows the high-efficiency potential of the combined SOFC-PEMFC system and highlights the interaction between SOFC and PEMFC. The PEMFC is influenced by changing the conditions upstream in the SOFC; however, because there is no physical feedback from the PEMFC to the SOFC, the PEMFC can be optimised independently of the SOFC. The hydrogen purification system presented herein is based on WGS reactors and a general separator. Details on the specific method or approach for trace CO and CO_2 removal are not included. As the choice of AOG post-treatment and purification method is beyond the scope of this research, this level of detail is deemed sufficient. However, in future research, the model should be expanded with a more detailed purification system to improve the credibility of the

Table 4: Percentage change in net electrical efficiency and fraction of total power produced by the PEMFC compared to nominal values as a function of x_{purge} and $u_{f_{PEM}}$.

Parameter	Nominal value	Set value	Percentage change $\eta_{el,AC}$ [%]	Percentage change $f_{P_{PEMFC}}$ [%]
x_{purge}	20	0	0.754	3.063
		10	0.353	1.396
		30	-0.342	-1.356
$u_{f,PEM}$	0.85	0.6	-1.774	-7.092
		0.7	-0.944	-3.770
		0.8	-0.282	-1.121
		0.9	0.257	1.032

proposed setup. Figures 3(a-c) show the invalid operating regimes (gray areas) to cover significant sections of the simulation matrix. This highlights the precarious balance between increasing the SOFC efficiency (reducing thermal losses) and retaining sufficient waste energy in the anode/cathode off-gas streams for preheating the different reactant flows. This shows the trade-off that must be made between optimising the design point efficiency and retaining a sufficiently large operating envelope.

6 FUTURE WORK

This work presents a basis for the comparison of the SOFC-PEMFC combined cycle with other SOFC-based combined cycle systems and different stand-alone SOFC system layouts. In future research, the purification step should be modeled in more detail, after which a more in-depth analysis can be performed, such as an investigation of exergy losses in the system. Moreover, the effects of using different alternative fuels other than methane will also be included in the next stage of this research. To do this, different fuel pre-processing models will be developed and included within the currently developed model. Moving forward, off-design conditions such as part-load operation will also be investigated to identify the operating envelope and operational constraints of the system.

ACKNOWLEDGEMENTS

This research is supported by the SH_2IPDRIVE project, which aims to accelerate the introduction of hydrogen as an alternative energy carrier in the Dutch maritime sector. The main goal is to develop reliable, safe, standardized, and scalable solutions for zero-emission propulsion and energy systems on board ships. The project is funded by the Rijksdienst voor Ondernemend Nederland (RVO) under the R&D Mobiliteitssectoren regulation.

REFERENCES

[1] IMO, "Fourth imo ghg study 2020 executive-summary," Report, 2020.

[2] IMO, "2023 imo strategy on reduction of ghg emissions from ships," Report, 2023.

[3] F. Baldi, S. Moret, K. Tammi, and F. Maréchal, "The role of solid oxide fuel cells in future ship energy systems," *Energy*, vol. 194, 2020, ISSN: 03605442.

[4] R. Payne, J. Love, and M. Kah, "Generating electricity at 60% electrical efficiency from 1-2 kwe sofc products," in *ECS Transactions*, vol. 25, pp. 231–239.

[5] A. C. Power, *Alma clean power announces breakthrough in direct ammonia fuel cells*, Web Page, 2023. [Online]. Available: `https://almacleanpower.com/news/alma-clean-power-announces-breakthrough-in-direct-ammonia-fuel-cells`.

[6] L. van Biert, M. Godjevac, K. Visser, and P. V. Aravind, "A review of fuel cell systems for maritime applications," *Journal of Power Sources*, vol. 327, pp. 345–364, 2016, ISSN: 03787753.

[7] B. N. van Veldhuizen, L. van Biert, P. V. Aravind, and K. Visser, "Solid oxide fuel cells for marine applications," *International Journal of Energy Research*, vol. 2023, p. 35, 2023.

[8] T. Tronstad, H. Hogmoen Astrand, G. Haugom, and L. Langfeldt, "Study on the use of fuel cells in shipping," European Maritime Safety Agency, Report, 2017.

[9] L. van Biert, T. Woudstra, M. Godjevac, K. Visser, and P. V. Aravind, "A thermodynamic comparison of solid oxide fuel cell-combined cycles," *Journal of Power Sources*, vol. 397, pp. 382–396, 2018, ISSN: 03787753.

[10] D. Cocco and V. Tola, "Externally reformed solid oxide fuel cell–micro-gas turbine (sofc–mgt) hybrid systems fueled by methanol and di-methyl-ether (dme)," *Energy*, vol. 34, no. 12, pp. 2124–2130, 2009, ISSN: 03605442.

[11] V. He, M. Gaffuri, J. Van herle, and J. Schiffmann, "Readiness evaluation of sofc-mgt hybrid systems with carbon capture for distributed combined heat and power," *Energy Conversion and Management*, vol. 278, 2023, ISSN: 01968904.

[12] F. D. F. Chuahy and S. L. Kokjohn, "Solid oxide fuel cell and advanced combustion engine combined cycle: A pathway to 70% electrical efficiency," *Applied Energy*, vol. 235, pp. 391–408, 2019, ISSN: 03062619.

[13] H. Sapra, J. Stam, J. Reurings, *et al.*, "Integration of solid oxide fuel cell and internal combustion engine for maritime applications," *Applied Energy*, vol. 281, 2021, ISSN: 03062619.

[14] A. Dicks, R. Fellows, C. Mescal, and C. Seymour, "A study of sofc-pem hybrid systems," *Journal of Power Sources*, vol. 86, pp. 501–506, 2000.

[15] L. J. Tan, C. Yang, and N. Zhou, "Performance of the solid oxide fuel cell (sofc)/proton-exchange membrane fuel cell (pemfc) hybrid system," *Chemical Engineering & Technology*, vol. 39, no. 4, pp. 689–698, 2016, ISSN: 09307516.

[16] X. Cheng, Z. Shi, N. Glass, *et al.*, "A review of pem hydrogen fuel cell contamination: Impacts, mechanisms, and mitigation," *Journal of Power Sources*, vol. 165, no. 2, pp. 739–756, 2007, ISSN: 03787753.

[17] Z. Wu, Z. Zhang, and M. Ni, "Modeling of a novel sofc-pemfc hybrid system coupled with thermal swing adsorption for h2 purification: Parametric and exergy analyses," *Energy Conversion and Management*, vol. 174, p. 802, 2018, ISSN: 0196-8904 0196-8904.

[18] E. Riensche, U. Stimming, and G. Unverzagt, "Optimization of a 200 kw sofc cogeneration power plant part 1: Variation of process parameters," *Journal of Power Sources*, vol. 73, pp. 251–256, 1998.

[19] B. N. van Veldhuizen, L. van Biert, A. Amladi, T. Woudstra, K. Visser, and P. V. Aravind, "The effects of fuel type and cathode off-gas recirculation on combined heat and power generation of marine sofc systems," *Energy Conversion and Management*, vol. 276, 2023, ISSN: 01968904.

[20] C. Stiller, B. Thorud, S. Seljebø, Ø. Mathisen, H. Karoliussen, and O. Bolland, "Finite-volume modeling and hybrid-cycle performance of planar and tubular solid oxide fuel cells," *Journal of Power Sources*, vol. 141, no. 2, pp. 227–240, 2005, ISSN: 03787753.

[21] A. Ghenciu, "Review of fuel processing catalysts for hydrogen production in pem fuel cell systems," *Current Opinion in Solid State nd Materials Science*, vol. 6, no. 5, pp. 389–399, 2002.

[22] E.-S. Bang, M.-H. Kim, and S.-K. Park, "Options for methane fuel processing in pemfc system with potential maritime applications," *Energies*, vol. 15, no. 22, 2022, ISSN: 1996-1073.

[23] F. de Bruijn, D. Papageorgopoulos, E. Sitters, and G. Janssen, "The influence of carbon dioxide on pem fuel cell anodes," *Journal of Power Sources*, vol. 110, pp. 117–124, 2002.

[24] A. de Groot, "Advanced exergy analysis of high temperature fuel cell systems," Thesis, 2004.

[25] P. V. Aravind, T. Woudstra, N. Woudstra, and H. Spliethoff, "Thermodynamic evaluation of small-scale systems with biomass gasifiers, solid oxide fuel cells with ni/gdc anodes and gas turbines," *Journal of Power Sources*, vol. 190, no. 2, pp. 461–475, 2009, ISSN: 03787753.

[26] N. Woudstra, T. van der Stelt, and K. Hemmes, "The thermodynamic evaluation and optimization of fuel cell systems," *Journal of Fuel Cell Science and Technology*, vol. 3, pp. 155–164, 2006.

[27] K. Hemmes, A. Patil, and N. Woudstra, *Internal reforming sofc system for flexible coproduction of hydrogen and power*, Conference Paper, 2005.